Active enhancement of synapse driven depolarization of perisynaptic astrocytic processes

Ryo J. Nakatani[1] and Erik De Schutter[1*]

[1]Computational Neuroscience Unit, Okinawa Institute of Science and Technology, 1919-1 Tancha, Onna Village, 904-0412, Okinawa, Japan.

*Corresponding author(s). E-mail(s): erik@oist.jp;
Contributing authors: ryo.nakatani@oist.jp;

Abstract

Electrophysiological properties underlie the fundamental mechanisms of the brain. Although astrocytes have typically been considered not electrically excitable, recent studies have shown depolarization of astrocytes induced by local extracellular potassium changes caused by neuronal activity. Interestingly, astrocytic depolarization is only induced within the periphery of the astrocyte, where astrocytes contact neurons. This depolarization affects the brain's information processing, as depolarization alters astrocyte functionality and neurotransmitter dynamics. However, specific mechanisms causing astrocytic depolarization have remained unknown due to the limitations of experimental techniques. Here, we construct a computational whole-cell astrocyte model containing experimentally verified astrocytic channels relevant to depolarization. Using our model, we suggest that previously reported potassium channels alone are insufficient for astrocyte depolarization and additional mechanisms are required. Our simulations show that NMDARs contribute to this depolarization by cooperating with Kir 4.1 to actively enhance extracellular potassium concentration and, thus, sustain depolarization.

Keywords: astrocytes; computational neuroscience; Kir 4.1; NMDAR; conductance-based models;

1 Introduction

The electrophysiological properties of brain cells are the foundation of information transfer within the brain. For the past century, neurons have been thought to be

the only cell type with these dynamic electrical properties. As dynamic changes in membrane potentials are how neurons propagate information, other non-neuronal cells, otherwise known as glia, were considered irrelevant to the brain's information processing.

Astrocytes, which account for more than half of glial cells in the human brain, have similarly shown passive responses to classical electrophysiological techniques. Within these electrophysiological studies, many have explored various manipulations that alter astrocyte membrane potentials, such as changing extracellular potassium concentrations or conducting knock-out (KO) of inwardly rectifying potassium 4.1 (Kir 4.1) channels, which results in an elevated resting membrane potential [1, 2]. However, few reports have considered that astrocyte membrane potential changes can trigger an active response in the astrocyte, which can provide feedback information to neuronal activity. Recent reports utilizing fluorescent voltage indicators show dynamic changes in astrocytic membrane potentials occurring only at the peripheral parts contacting synapses [3]. These contact sites between astrocytes and synapses, called perisynaptic astrocytic processes (PAPs), are where the astrocyte modulates neurotransmission. This astrocytic depolarization observed in the periphery is thought to be caused by membrane potential changes at PAPs responding to extracellular potassium elevation induced by action potentials [3, 4]. Interestingly, the depolarization of PAPs contributes to the increase of glutamate spillover [5, 6]. The spillover strongly affects synaptic responses in local neighboring synapses, potentially affecting brain computation.

This raises the possibility of an astrocyte-initiated active response to neuronal activity. However, it is still unclear if these potassium-mediated depolarizations are feasible under physiological conditions because previous studies estimated they require a minimum of 10 mM of extracellular potassium [3]. As potassium can diffuse to nearby synapses as well as be taken up by postsynaptic potassium-chloride cotransporter 2 (KCC2) channels, maintaining such a high concentration is thought to be difficult [7]. The specific mechanisms causing PAP depolarization remain largely unknown, with only major astrocyte channels such as Kir 4.1 and excitatory amino-acid transporter (EAATs) examined [3]. This lack of experimental data, along with experimental limitations preventing direct observation of PAPs, causes the necessity of computational approaches. The use of mathematical models allows to theoretically explore the full extent of astrocyte membrane potentials. Although previous studies have also constructed astrocyte mathematical models that simulate electrophysiological data [8, 9], none of these models have focused on how PAP depolarization can be triggered and contained locally.

In this study, we constructed an empirical conductance-based NEURON model with a realistic morphology in order to capture both PAP and whole astrocyte properties. The constructed model contained potassium and glutamate receptors as well as transporters in order to compare with experimental results. This differentiated our model from more simplistic astrocyte depolarization models [9], as morphology affects electrophysiological responses. Through deciphering currents recorded in our mechanistic model, we observed that the amplitude of depolarization was controlled by the

continuous rise in extracellular potassium induced by Kir 4.1 efflux, which was sustained by N-methyl-D-aspartate receptor (NMDAR) inward currents. This cooperation between channels allow for astrocytic depolarization to be achieved in physiological ranges of action potential mediated extracellular potassium increases, below concentrations that were previously estimated. Our model provides a crucial hypothesis on active regulation of PAP depolarization, which may have strong influences on neurotransmitter diffusion.

2 Results

2.1 Kir 4.1 induces focal depolarizations dependent on extracellular potassium in astrocytes

We constructed an astrocyte potassium whole-cell model to examine the interaction between potassium and membrane potentials of an astrocyte. The constructed conductance-based model contained the major contributors of potassium, using a previously reported whole-cell morphology [8] (Fig. 1a,c). This morphology contained astrocyte nanoscopic structures that recreate characteristics of PAPs, such as the high input resistance (Supplementary Fig. 1). To validate our model, we tested the astrocyte response to dual patch clamp protocols, which showed passive responses as reported [10] (Fig. 1b). The model exhibited a hyperpolarized resting membrane potential (RMP) between -80 $\sim$ -85 mV, which is another defining characteristic of astrocytes [11].

We next used our model to examine the order of extracellular potassium necessary for potassium-dependent depolarization of $\sim$ 20 mV. In our initial experiments, we showed that at least a 10 mM extracellular increase of potassium at the PAP is necessary for a peak depolarization over 10 mV (Fig. 1d,g-i). This showed that in order to match experimental depolarizations of 20 mV, higher concentrations of extracellular potassium were necessary. We matched experimental values of peak PAP depolarization [3], which revealed that $\approx$ 43 mM of potassium was necessary to match experimentally measured results, substantially higher than the initially proposed 10 mM (Supplementary Fig. 2). The depolarization was also seen to be confined to the PAP, as a strong voltage attenuation (space constant 4.56 µm) occurs with a minimal voltage change at the soma (Fig. 1e). To gauge the extent of potassium-dependent depolarization, we next tested the model with various concentrations of extracellular potassium stimuli and Kir 4.1 densities. The results showed a strong potassium dependence, with high potassium concentrations and Kir 4.1 densities required for significant depolarizations (Fig. 1f).

As the previous results showed a strong dependence on relatively high potassium concentrations and Kir 4.1 densities, we checked whether this was possible in the physiological range. To examine whether PAP depolarization is possible in physiological conditions, we applied simplified action potentials (sAP; 0.5 mM increase of extracellular potassium for 0.5 ms) for 10 pulses at 100 Hz. This protocol was chosen to match the stimuli protocol from previous experiments [3]. The potassium change caused by a single action potential (AP) was estimated using values from previous computational

models of potassium in the synaptic cleft [7, 12]. Potassium from postsynaptic neuronal α-amino-3-hydroxy-5-methyl-4-isoxazolepropionic acid receptor (AMPAR) and N-methyl-D-aspartate receptor (NMDAR) activity was regarded as negligible for distances of astrocytes from the postsynaptic density (PSD) [13]. As the repolarization process of neurons typically lasts 0.5 ms, a period of 0.5 ms was chosen. This resulted in minimal depolarizations that do not match experimental values, as there is no potassium build-up within the extracellular space at the PAP (Fig. 1f, Supplementary Fig. 2). Therefore, we hypothesize that Kir 4.1 alone is insufficient for PAP depolarization in conditions using physiological stimulation of single synapses.

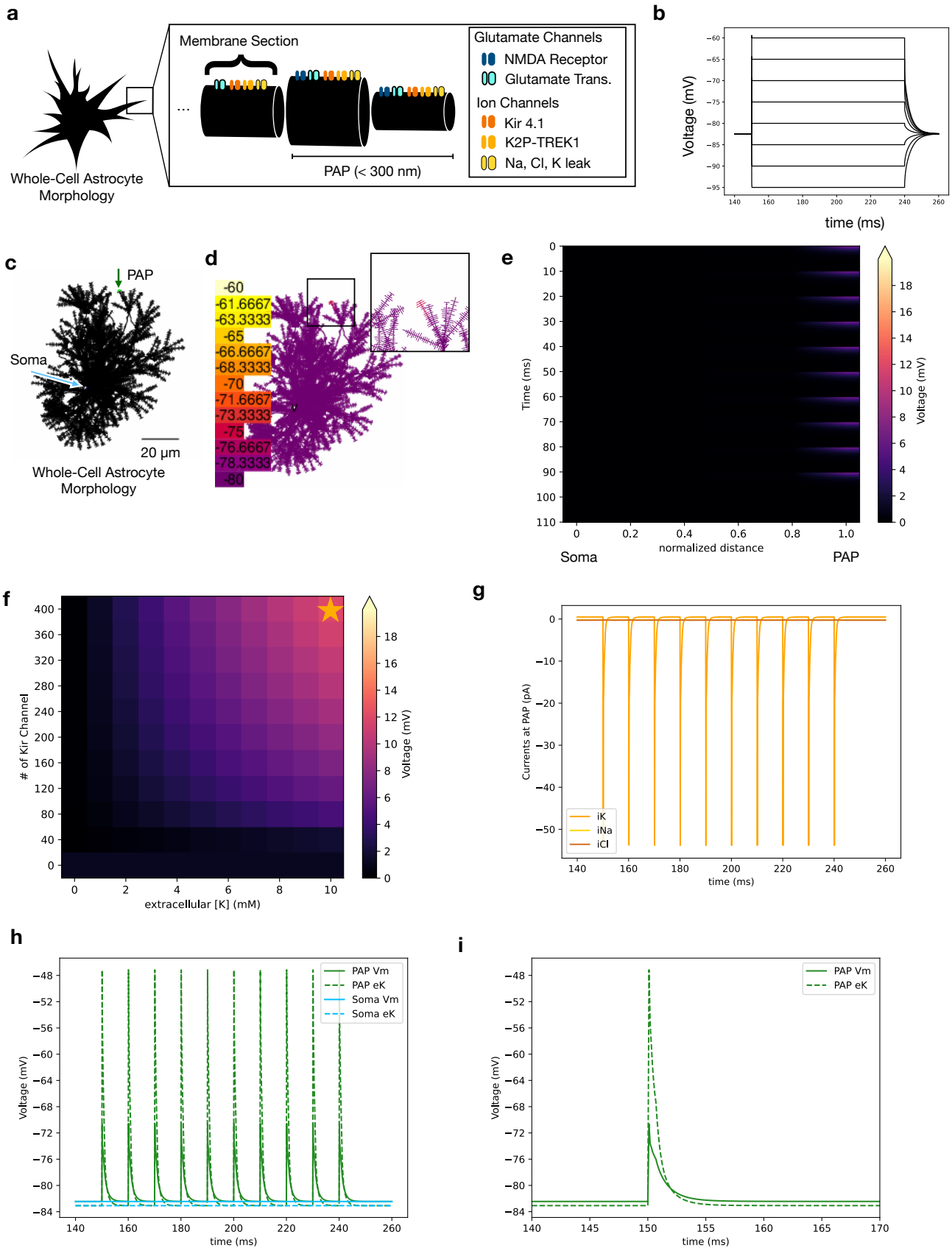
a
Membrane Section
Glutamate Channels
NMDA Receptor
Glutamate Trans.
Ion Channels
Kir 4.1
K2P-TREK1
Na, Cl, K leak
PAP (< 300 nm)
Whole-Cell Astrocyte Morphology
b
Voltage (mV)
time (ms)
c
PAP
Soma
20 µm
Whole-Cell Astrocyte Morphology
d
e
Time (ms)
normalized distance
Soma
PAP
Voltage (mV)
f
# of Kir Channel
extracellular [K] (mM)
Voltage (mV)
g
Currents at PAP (pA)
iK
iNa
iCl
time (ms)
h
PAP Vm
PAP eK
Soma Vm
Soma eK
Voltage (mV)
time (ms)
i
PAP Vm
PAP eK
Voltage (mV)
time (ms)

Fig. 1 The whole-cell astrocyte model

a, Cartoon depicting our conductance-based model. The astrocyte morphology is that of a previously constructed model [8], with Kir 4.1, K2P-TREK1, and glutamate transporters (GluTs). Only sections within the first 300 nm of the peripheral astrocyte are considered a PAP and contain the NMDAR. Each cylinder in the cartoon represents a cable section of the astrocyte model. **b,** The soma voltage response to various voltage clamps. Voltage commands are to -95 $\sim$ -65 mV with 5 mV increments. **c,** The whole-cell morphology of the astrocyte previously described in Savtchenko et al. [8]. The scale bar shows 20 µm. **d,** Depolarization visualized at the peak in our whole-cell astrocyte model. The colors indicate the membrane potential of each compartment and correspond to the color scale within the figure. A closer view of the first peak in the stimulated PAP is visualized within the window. The depolarization is induced with 400 Kir channels on PAP and 10 mM of extracellular potassium. **e,** The voltage attenuation along the branch from PAP to Soma. Distance is normalized to the distance of the PAP from the soma. The depolarization is induced with 400 Kir channels on PAP and 10 stimuli of 10 mM of extracellular potassium at 10 ms intervals. **f,** Potassium dependence of model. Increases of extracellular concentrations have been tested for ranges of 0 to 10 mM, compared to various counts of Kir 4.1 on the PAP. The star indicates the parameter combination used in d,e,g,h,i. **g,h, (g)** Currents, **(h)** Voltage response to 10 stimuli of 10 mM increase for 0.5 ms. 400 Kir channels on the PAP without any glutamate stimuli. **i,** A closer examination of a single response for voltage responses in h from 10 ms before the stimulus to 20 ms after.

2.2 Minimal NMDAR lead to extracellular potassium independent depolarization

As previous results show, potassium build-up in the extracellular space with APs and astrocyte channels alone is difficult. Next, we examined astrocytic channels with sustained currents activated with potassium or glutamate from the AP. As recent reports imply the functional expression of NMDAR on the astrocyte and at the PAP [14–16], we examined the effects of these channels on PAP depolarization. As sub-compartment proteomes of tripartite synapses show a lack of NMDAR [17] as well as many reports contradicting the expression of astrocytic NMDAR [18, 19], we hypothesize that these channels are expressed at a much lower density than Kir 4.1 channels, making them difficult to detect with conventional methods.

To observe the effects of NMDAR, we implemented a previously reported NMDAR model [20] with low density on the PAP. We next examined the peak depolarization in the PAP by adding 1 mM glutamate after the potassium stimulus. Using the same 10 pulse 100 Hz stimulus of this sAP, we observed peak depolarizations of ≈ 21 mV that match experimental results (Fig. 2a, Supplementary Fig. 3). Although the depolarization was sustained for longer than that of Kir 4.1 only, voltage attenuation maintained the isolation of PAP voltage dynamics (Fig. 2b). This isolation was maintained regardless of the number of PAPs simultaneously triggered, with activation of 10 PAPs resulting in a < 1 mV change at the soma (Supplementary Fig. 4). We also observed a loss of potassium dependence, as NMDAR is a glutamate-triggered inward current (Fig. 2c).

To understand this change in potassium dependence, we examined the changes in extracellular potassium and potassium currents relative to voltage changes. This revealed two contributions of the NMDAR to larger depolarizations. First, we found the interaction between NMDAR and Kir 4.1 contributed to a continuous outward potassium flow, which raised the extracellular potassium concentrations to levels not achieved by Kir 4.1 alone. The second contribution of NMDAR on PAP depolarization is from the longer channel open time, which allows for a build-up between stimuli (Fig. 3a,b).

These contributions allow for a steady increase in the extracellular potassium concentrations, affecting potassium reversal potential (eK). Interestingly, we also identified the importance of eK to NMDAR depolarization amplitude by examining how much depolarization can be achieved under an arbitrary constant extracellular potassium concentration (i.e., eK). As a result, we observed that an eK of -70 mV is necessary for maximum depolarization amplitude (Fig. 2d). This implies that increasing extracellular potassium concentrations to 5.68 mM is necessary for maximum depolarization.

We also examined the effects of glutamate transporters (GluT), as they have been experimentally identified to be a candidate that can contribute to depolarization [3]. However, the increase in extracellular potassium and channel open times was smaller than that of the NMDAR channel, resulting in minimal contributions to depolarization (Supplementary Fig. 5).

Summarizing our previous results, we observed a complex interaction scheme between Kir 4.1 and NMDAR, which produces a depolarization triggered by potassium

and glutamate. In this scheme, boosting extracellular potassium by the competition between NMDAR and Kir 4.1 is crucial for boosting depolarization compared to the original 0.5 mM extracellular potassium increase. Initially, in the steady state with no excessive extracellular potassium, the Kir 4.1 channel produces a weak outward current that balances sodium and chloride leak currents (Fig. 3c1). However, the eK is altered upon an increase in extracellular potassium. Kir 4.1 produces a strong instantaneous potassium-dependent inward current, pushing the membrane potential to that of the new eK (Fig. 3c2). As the application of glutamate follows the potassium stimulus, this triggers the NMDAR to activate, pushing the membrane potential over the eK and reverting Kir 4.1 back to an outward current that increases extracellular potassium (Fig. 3c3). This depolarization and accumulation of extracellular potassium continue while the NMDAR current is stronger than the Kir 4.1 outward current (Fig. 3c4). Eventually, the time course of depolarization follows the interplay between the NMDAR inward current and Kir 4.1 outward current (Fig. 3c4,c5) until the next stimulus triggers an additional extracellular potassium increase (Fig. 3c2). Our results suggest that activating NMDAR is crucial in obtaining physiological PAP depolarizations.

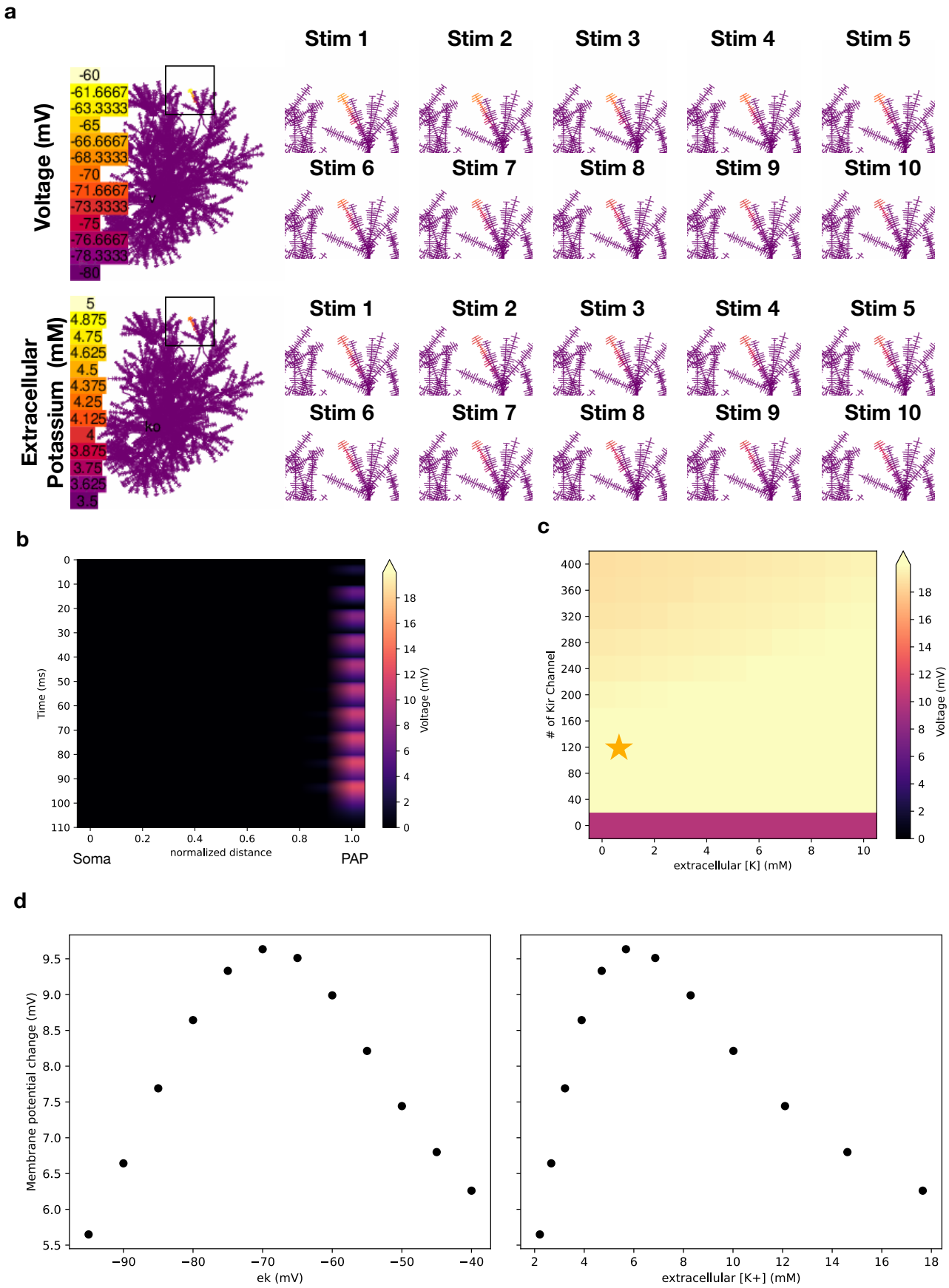
a
Stim 1
Stim 2
Stim 3
Stim 4
Stim 5
Stim 6
Stim 7
Stim 8
Stim 9
Stim 10
Voltage (mV)
-60
-61.6667
-63.3333
-65
-66.6667
-68.3333
-70
-71.6667
-73.3333
-75
-76.6667
-78.3333
-80
Extracellular Potassium (mM)
5
4.875
4.75
4.625
4.5
4.375
4.25
4.125
4
3.875
3.75
3.625
3.5
b
Time (ms)
Voltage (mV)
Soma
normalized distance
PAP
c
# of Kir Channel
extracellular [K] (mM)
Voltage (mV)
d
Membrane potential change (mV)
ek (mV)
extracellular [K+] (mM)

Fig. 2 Glutamate response of the whole-cell astrocyte model

a, Depolarization and extracellular potassium visualized at the peak in our whole-cell astrocyte model with activation of NMDAR. The colors indicate the membrane potential/extracellular potassium of each compartment, corresponding to the color scale within the figure. A closer view of the stimulated PAP is visualized on the right corresponding to the window in the whole-cell. Each zoomed view shows the response to each stimuli of the 100 Hz 10 stimulus protocol. Decreased Kir 4.1 numbers to 120 and extracellular potassium to 0.5 mM compared to figure 1d. **b,** The voltage attenuation along the branch from PAP to Soma. Distance is normalized with the distance from the PAP to the soma. **c,** Potassium dependence of model. Increases of extracellular concentrations have been tested for ranges of 0 to 10 mM, compared to various counts of Kir 4.1 on the PAP. The star indicates the parameter combination used in a,b and in Fig. 3. **d,** Maximum membrane potential changes achieved under various extracellular potassium bath conditions. Extracellular bath conditions are computed as reversal potential (ek) for the model and plotted as Left) ek against membrane potential change, Right) extracellular potassium bath condition against membrane potential change.

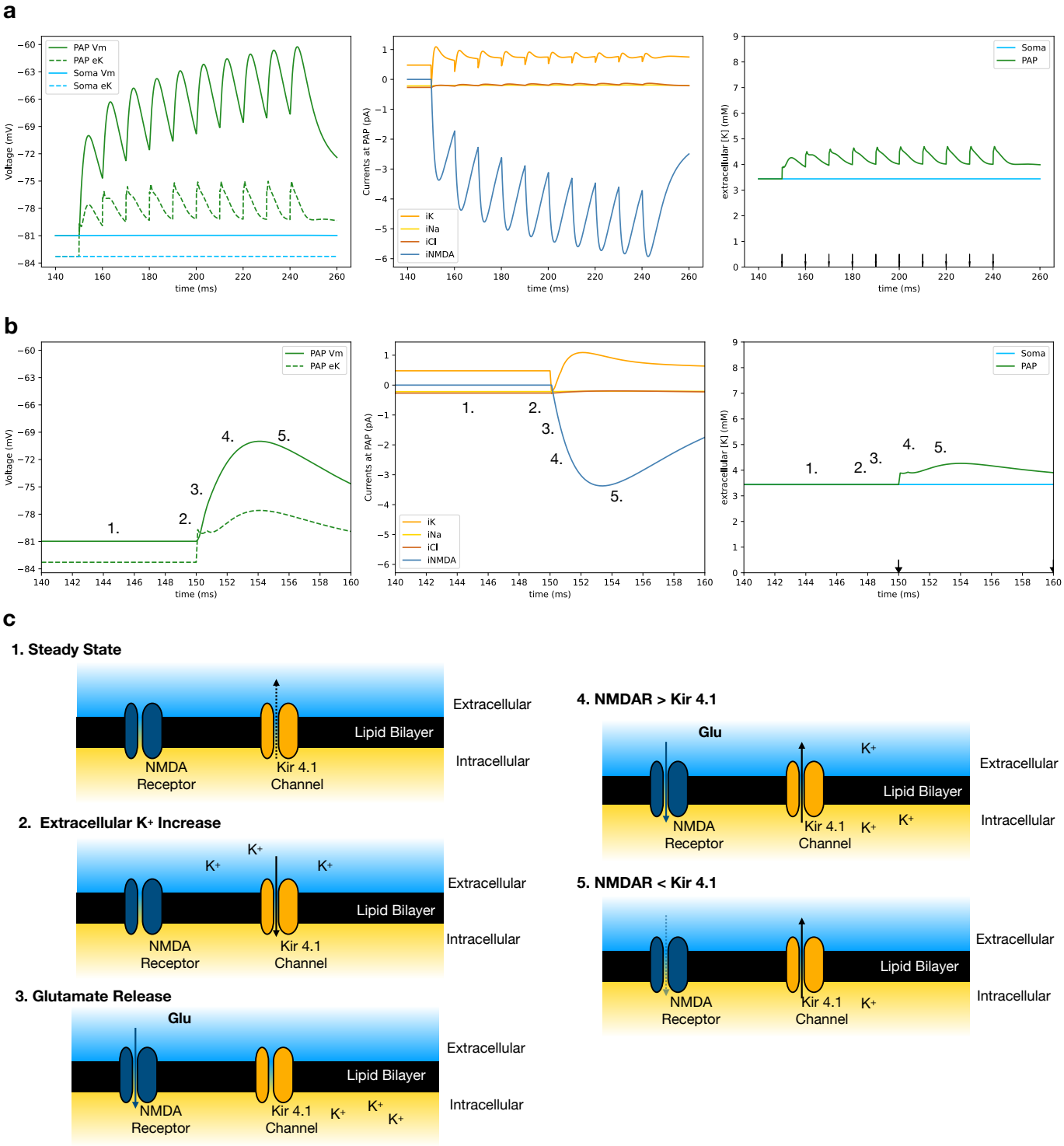
a
PAP Vm
PAP eK
Soma Vm
Soma eK
Voltage (mV)
time (ms)
Currents at PAP (pA)
iK
iNa
iCl
iNMDA
Soma
PAP
extracellular [K] (mM)
b
1.
2.
3.
4.
5.
c
1. Steady State
Extracellular
Lipid Bilayer
Intracellular
NMDA Receptor
Kir 4.1 Channel
2. Extracellular K+ Increase
K+
3. Glutamate Release
Glu
4. NMDAR > Kir 4.1
5. NMDAR < Kir 4.1

Fig. 3 PAP depolarization mechanisms

a, The recorded Left) voltage change along with eK Middle) currents Right) extracellular potassium concentration within the tip of the PAP section for the simulation shown in Fig. 2a. **b,** 10 ms before and after the first stimulation in a. **c,** The cartoon depicts the direction of currents for Kir and NMDAR channels throughout the initial depolarization. All NMDAR currents are dark blue, and potassium currents are colored black. Dashed lines represent smaller currents. The cartoon depicts 5 stages that contribute to depolarization and repolarization. The respective stages are numbered in b.

2.3 Balance between NMDAR and Kir 4.1 determines depolarization dynamics

We next examined how altering the channel balance between NMDAR and Kir 4.1 contributes to peak depolarization in both single stimulus and 10 stimuli protocols. This comparison shows that the NMDAR density mainly controls the depolarization peak, although Kir 4.1 overexpression lowers depolarization amplitudes (Fig. 4a). So, how does the balance between Kir 4.1 and NMDAR currents change in each condition? We highlight three conditions relative to the control condition, where we increase either the Kir 4.1 density to 400 channels, the NMDAR to densities matching neuronal PSDs (25 channels) [21], or both. By increasing NMDAR from (Fig. 4b) to (Fig. 4c) we increased the peak depolarization by 20 mV. On the contrary, increasing Kir from (Fig. 4c) to (Fig. 4d) lowered the peak depolarization by 5 mV.

To further analyze how each channel contributes to depolarization dynamics, we examined the phase plane of extracellular potassium against membrane potential. This revealed how each channel affected the depolarization dynamics of astrocytes (Fig. 4e). The primary changes caused by increasing NMDAR are large increases in potassium concentration and membrane potential, specifically seen as a loop structure in the upper left of the phase plane (Fig. 4e; left vs. right). On the other hand, the consequence of increasing Kir 4.1 was a stronger attraction to eK (Fig. 4e; top vs. bottom). Therefore, our results suggested that the Kir 4.1 channel and NMDAR balance strongly determines the depolarization dynamics.

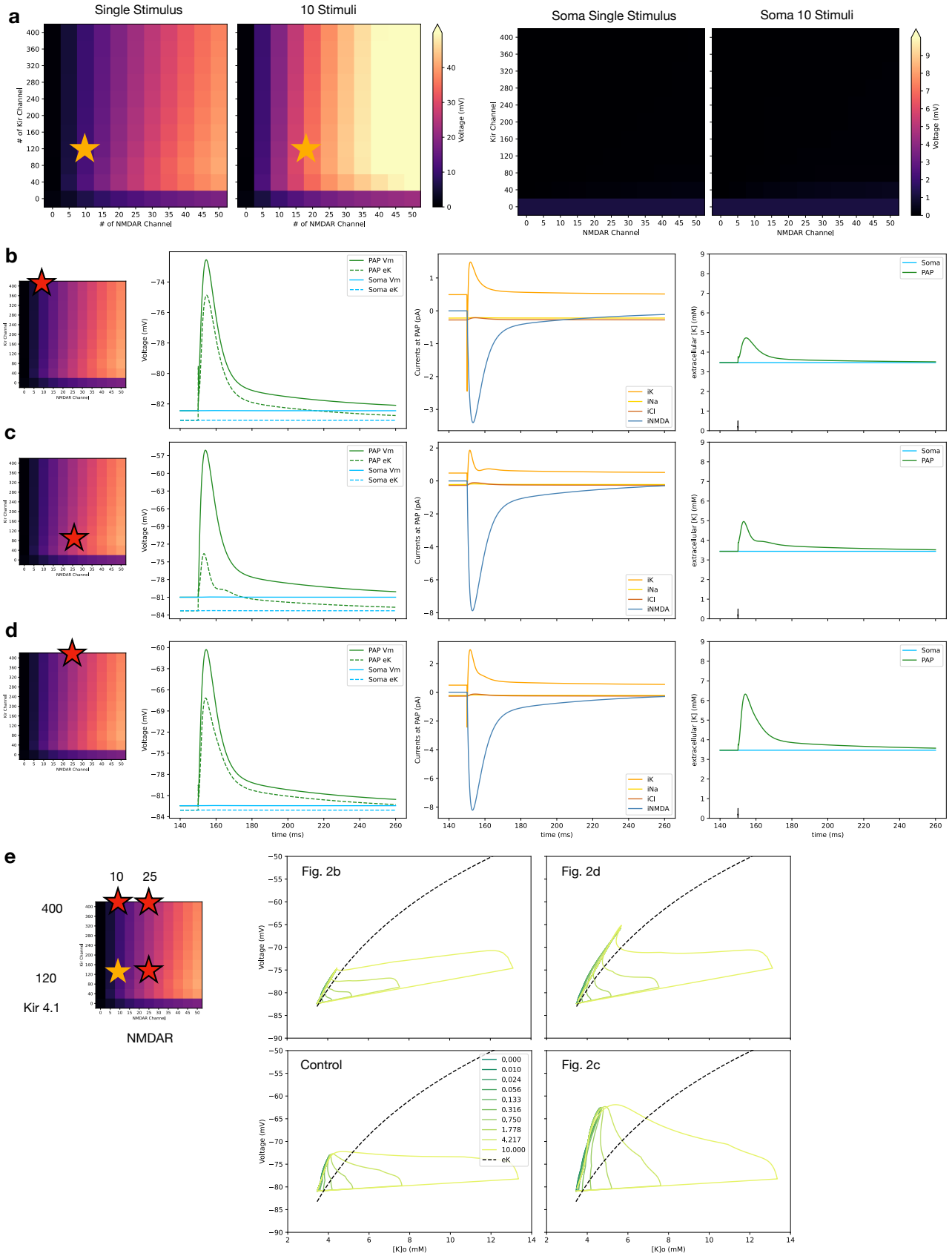
a
Single Stimulus
10 Stimuli
Soma Single Stimulus
Soma 10 Stimuli
# of Kir Channel
# of NMDAR Channel
Kir Channel
NMDAR Channel
Voltage (mV)
b
c
d
PAP Vm
PAP eK
Soma Vm
Soma eK
Voltage (mV)
Currents at PAP (pA)
iK
iNa
iCl
iNMDA
Soma
PAP
extracellular [K] (mM)
time (ms)
e
10
25
400
120
Kir 4.1
NMDAR
Fig. 2b
Fig. 2d
Control
Fig. 2c
0,000
0,010
0,024
0,056
0,133
0,316
0,750
1,778
4,217
10,000
eK
[K]o (mM)

Fig. 4 A comparison of various channel counts to peak depolarization

a, Heat maps showing maximum depolarization for each count of Kir 4.1 channels and NMDAR channels on the PAP. The heat-map shows peak depolarization recorded at the Left) PAP Right) Soma for single and 10 stimuli. The star indicates the parameters used for previous depolarization results in Figures 2 and 3. **b-c,** Heat map with a star showing parameters used, Left) voltage change along with reversal potential (eK), Middle) currents, Right) extracellular potassium concentration within the tip of the PAP section. The parameters (Kir:NMDAR) are **(b)** (120:10) **(c)** (120:25) **(d)** (400:25). **e,** Phase planes of [K]o vs. voltage for respective combinations of Kir: NMDAR. Left) The heat map shows the parameters used to draw phase planes. Right) respective phase planes for each condition.

2.4 Potassium and glutamate spillover contribute to depolarization

So far, we have examined depolarization caused by a single synapse but have neglected the importance of local contributions to neighboring synapses [3, 7, 22]. As the stimuli protocols we use in our experiments will alter neighborhood glutamate and potassium concentrations [3, 7], we next examined how the leakage of potassium and glutamate from the synaptic cleft would affect astrocyte depolarization.

Here, we use a simplified model of local spillover of potassium and glutamate by increasing the affected PAP length and examined peak depolarizations for various affected lengths in our conductance-based model. As a consequence, we did not consider 3-dimensional aspects of extracellular diffusion. We found that peak depolarization amplitudes increased by spillover up to a peak length of 1.47 µm (Fig. 5a). This amplitude change was due to changes of sustained depolarization between stimuli (Fig. 5b). By examining the currents for different affected PAP lengths, we saw that the initial depolarization is amplified due to the increase in active Kir 4.1 channels and NMDARs up to a certain threshold (Fig. 5b). On the other hand, at much longer distances like 10 µm, the balance between NMDAR and Kir 4.1 currents had reversed, thus causing a strong dampening effect on the depolarization (Supplementary Fig. 6).

As we described in Fig. 4, this change in balance controls depolarization amplitude. We next examined how changing Kir 4.1 densities affected this property. As previously reported, experimental over-expression or inhibition of Kir 4.1 was seen to decrease and amplify depolarization amplitudes, respectively [3]. Therefore, we aimed to see if our model could replicate this property. By comparing depolarization amplitude measured over various randomly selected PAPs between these various Kir 4.1 expression profiles, we see significant changes between each condition for both confined and spillover (Confined ANOVA p-value:4.15E-51, Spillover ANOVA p-value:2.30E-62; Fig. 5c). Confined conditions matched relationships seen in experiments, where means of Kir over-expression and inhibition were both significantly different from control(Control-OE t-test p-value:3.70E-8; Control-inhibition t-test p-value: 9.39E-12).

As a result, we saw a significant change between spillover and constrained conditions from Kir 4.1 (Paired t-test p-value:4.18E-15 Fig. 5c). This is due to the stronger potassium current activated at the PAP. GluT did not significantly alter depolarization in a spillover-dependent manner (Supplementary Fig. 7). In summary, these results highlight the importance of local spillover in enhancing PAP depolarization.

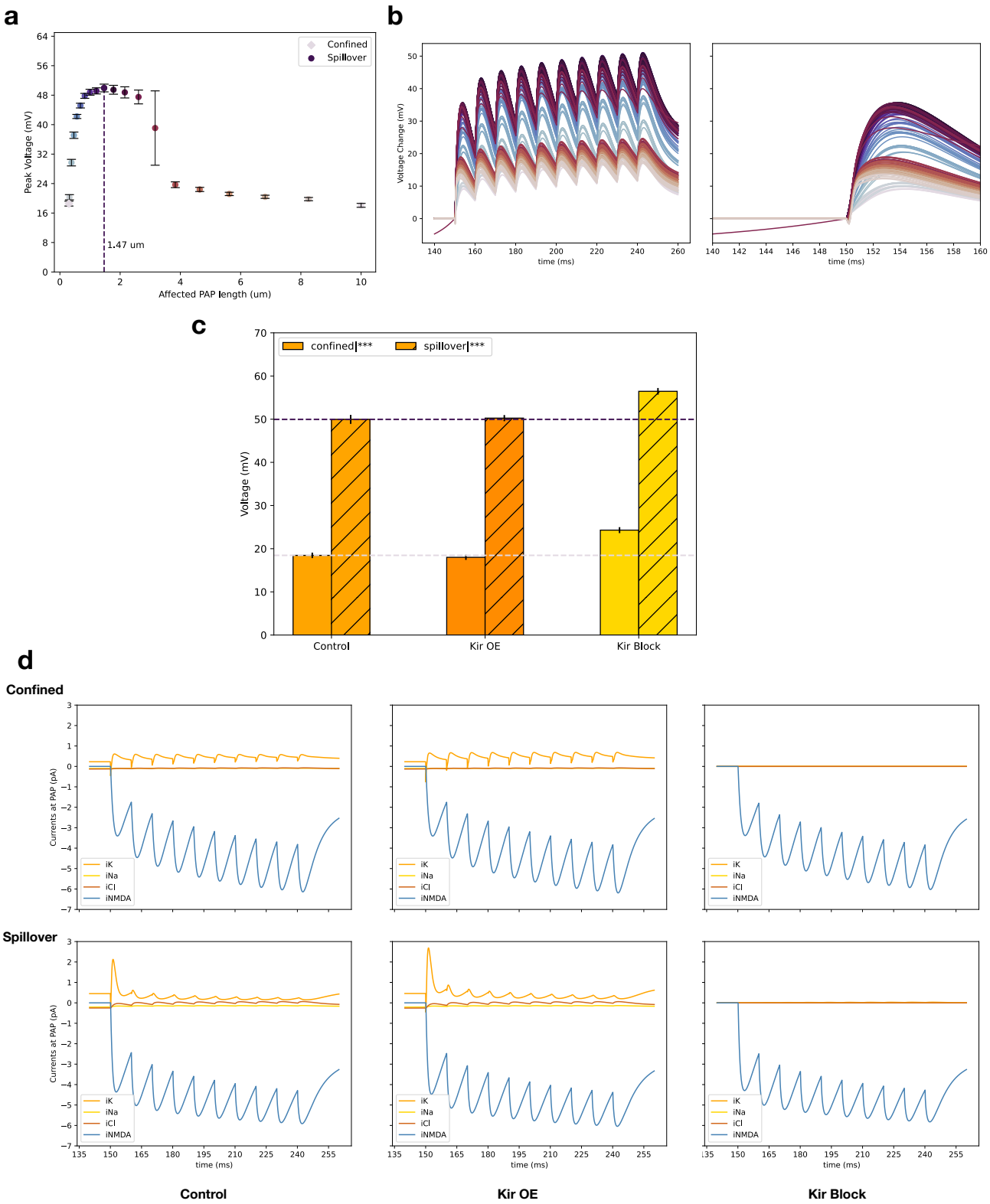
a
Confined
Spillover
Peak Voltage (mV)
1.47 um
Affected PAP length (um)
b
Voltage Change (mV)
time (ms)
time (ms)
c
confined***
spillover***
Voltage (mV)
Control
Kir OE
Kir Block
d
Confined
Spillover
Currents at PAP (pA)
iK
iNa
iCl
iNMDA
time (ms)
Control
Kir OE
Kir Block

Fig. 5 Spillover effect on PAP depolarization

a,b, Comparison of peak depolarization caused by spillover over various PAP lengths. **(a)** Plots of peak depolarization against PAP lengths. The diamond shown in the plot and legend indicates the confined conditions used to generate plots in c. Longer lengths than the confined conditions are all spillover conditions which are marked with a circle. n=10 for randomly selected PAP locations. The length for the peak depolarization is marked on the x-axis with its PAP length value (1.47 µm). The length for peak depolarization which was used for subsequent spillover conditions. The confined condition matches all parameter settings of depolarization in Fig. 2. **(b)** Left) Traces of membrane potential change over time. The color of each trace corresponds to the distance of the same color plot in a. Right) The same traces of membrane potential change in a time window of 20 ms around the stimulus. n=10. **c,** Effects of changing Kir 4.1 densities and PAP lengths on the peak depolarization. The spillover condition is the PAP length with peak depolarization indicated in a. The confined condition is the control PAP length. The bar plot indicates changes in Kir 4.1 with 120 Kir 4.1 for control, 0 for Kir 4.1 Block, and 168 for Kir 4.1 OE. Comparison between the Kir 4.1 densities shows significant differences between spillover (ANOVA p-value: 2.30E-62, n=10 for each Kir 4.1 density) and confined (ANOVA p-value: 4.15E-51, n=10 for each Kir 4.1 density) conditions. All Kir densities and NMDAR KO significantly differ between spillover and confined conditions (paired t-test p-values in Supplementary table 7, n=10). p-value 0.05 > *, 0.01 > **, 0.001 > ***. **d,** Plots of PAP recorded currents for various Kir 4.1 densities. Top) Confined conditions, Bottom) Spillover conditions for marked PAP length in a.

3 Discussion

This study focused on elucidating the mechanisms responsible for astrocyte peripheral depolarization using an empirical conductance-based mathematical model. We believe this study presents, for the first time, a robust mechanism explaining the process of PAP depolarization. Our model showed that although Kir 4.1 alone can depolarize the PAP, it required ≈ 43 mM of potassium in the extracellular space, which is an exceptionally high concentration that is physiologically difficult to achieve (Supplementary Fig. 2). Additionally, we showed that the initial potassium uptake mode by Kir 4.1 is inverted by the activation of NMDAR, which allows for depolarization to occur in ranges of physiological stimuli. This change from conventional Kir 4.1 uptake mode to potassium efflux mode drives the reversal potential to rise and controls the depolarization amplitude. The physiological implications of Kir 4.1 efflux are also thought to be important, as shown by the sustained outward currents in our model. An increase in extracellular potassium drives the astrocyte's depolarization and enhances neuronal activity, as neuronal excitability tightly depends on the extracellular potassium concentration [23].

Previous reports [3] showed that the mean astrocyte peak depolarization is not altered by applying the NMDAR antagonist APV and AMPAR antagonist DQNX. This phenomenon was not observed in our model which requires activation of a small number of NMDA channels for sustained large depolarization (Figs. 2-3, Supplementary Fig. 7). The discrepancy may be due to differences in astrocyte NMDAR subunit composition as certain NMDAR subunits are less susceptible to APV [24], which may also account for reports on astrocyte NMDA-induced, APV insensitive currents [25, 26]. The low and heterogeneous expression of astrocytic NMDAR has been discussed previously [27, 28]. More recent confirmation is provided by studies showing that knockdown of astrocytic NMDARs affects brain computation [14, 29]. Likewise, our model did not show any dependence of glutamate transporters for PAP depolarization, which was previously reported [3]. As GluT have strong voltage-dependent uptake [6], which was also seen in our model (Supplementary Fig. 8), it seems that a more detailed, glutamate-focused depolarization model may be necessary to simulate the interaction between depolarization and GluTs better.

PAP depolarization may strongly affect astrocytic function in information processing [3]. However, the extent to which the mechanism affects brain computation is unknown. The prevailing assumption is that astrocyte computation is done through increases of intracellular calcium [30]. Although, at first glance, PAP depolarization may seem to drive calcium influx, we believe depolarization does not directly contribute to regulating calcium concentrations. This is because voltage-dependent calcium channels (VDCC) on astrocytes (L-type, T-type, N-type, R-type) have high voltage thresholds that are difficult to achieve with ranges of depolarization shown experimentally [3] and in the model [31]. Previous experimental results match this description, where astrocyte L-type VDCC mediated influx required extracellular potassium levels of 75 mM, expected to cause large membrane depolarization [1]. Additionally, astrocytic NMDARs have lower calcium permeability than neuronal NMDARs, suggesting NMDAR-mediated depolarization does not drive large calcium influx in astrocytes [32]. However, voltage changes may affect local morphology

through changes in Aquaporins 4 voltage/potassium dependent water uptake [33, 34]. Interestingly, these AQP4 channels are coupled to Kir 4.1 channels, allowing for local morphological changes as a response to Kir 4.1 activity [35]. As changes in nanoscopic morphology are known to affect calcium dynamics within the PAP, this may be an indirect way to alter calcium responses [36].

Our current findings suggest that PAP depolarization is caused by the interaction between astrocytic NMDAR and Kir 4.1 channels. Utilizing a potassium-focused, astrocyte whole-cell conductance-based model, we showed this interaction can occur in physiological ranges of potassium and glutamate stimuli. These concentration ranges are much lower than initially anticipated by previous reports [3]. As the impact of PAP depolarization on synaptic plasticity is still unknown, further investigation into the properties of glutamate diffusion at the nanoscopic spatial scale is required.

4 Methods

Morphology

The morphology used in this model has been taken from a previously reported model [8], which includes peripheral, primary branch, and somatic structures. The model morphology is defined in NEURON [37], in the file GeometryAstrocyteCA1.hoc.

Channel Models

All subsequent channel models were defined in NEURON MODL. All parameters used in the model are listed in the Supplementary tables 1-6. Any alteration of channel counts were done by altering the single channel conductance linearly. Kir 4.1, GluT, TREK-1, leak channels were uniformly distributed for all simulations based on the channel counts defined in the PAP. As NMDAR channels have been seen to be confined to fine processes [38], NMDAR channels were placed in a Gaussian-distribution manner, with the farthest peripheral containing the most channels with units of PAP length 0.3 µm. Kir 4.1 channel numbers for OE and block conditions were matched with the experimental results in Armbruster et al. [3].

Kir 4.1

The Kir 4.1 channel model is adapted from Yim et al. [39] with a $[K^+]_o$ dependent square-root law [40].

$$g_{\text{Kir}} = g_{\text{Kir0}}\sqrt{[K^+]_o}$$

where g_{Kir0} is the maximum conductance. Maximum conductance was calculated to fit single-channel recordings and extracellular potassium concentrations of that experiment [41]. Specific changes are detailed in the Kir2.mod file and supplementary information.

NMDAR

The NMDAR model is adapted from Moradi et al. [20] with a few alterations to fit astrocyte NMDAR recordings. First, the voltage dependence of time constants for

the NMDAR model has been refit to that of astrocyte NMDAR recordings by [42]. Second, the magnesium dependence of the model was reduced, as astrocyte NMDAR currents are independent of extracellular magnesium concentrations [42]. Third, the induced glutamate concentration affects the model in a Hill equation-dependent manner, reducing activation when there is a low concentration of released glutamate. Last, the maximum conductance for single channel conductance was calculated from Jahr et al. [43]. Specific changes are detailed in the SynExp5NMDA.mod file and supplementary information.

K2P-TREK1 channel

The GHK-dependent rectification type potassium channel equations were taken from Janjic et al. [9]. These equations were converted into NEURON and observed to produce the same IV relationships mentioned in the original paper. Specific changes are detailed in the TWIK.mod file and supplementary information.

Glutamate Transporter

The glutamate transporter model was taken from that used in Savtchenko et al. [8] and modified from a membrane mechanism to a point process. Specific changes are detailed in the GluTrans.mod file and supplementary information.

Leak channels

Leak channels for Na^+,Cl^- were modeled as generic conductance-based channels with a predetermined conductance. The ratio of conductance between Na^+ and Cl^- was chosen based on previous models [9, 44]. The specific conductance value was arbitrarily fit, so the resting membrane potential was at -80 mV when Kir channel counts were 100 on the astrocyte PAP. The Kir channel count was calculated to fit the estimated minimum Kir 4.1 channel density on the astrocyte [45].

Chloride concentration was determined as the total sum of sodium and potassium concentration to maintain the extracellular charge, which was then used to calculate the reversal potential of the chloride leak channel. All leak files are defined as [ion name]leak.mod, where ion names are cl, k, or na.

Ion current to concentration conversion

The ion flux from intracellular to extracellular compartments is calculated with the conversion,

$$J_{\text{channel}} = \frac{I_{\text{channel}}}{F \times \text{Vol}_{\text{compartment}}}$$

where J, I describe the flux and current of any channel, F is the Faraday constant and Vol is the volume of the compartment. For potassium and sodium, this is modeled as a NEURONMODL file that follows chapter 9 of the NEURON book [37], modeling Ca^{2+} extracellular concentrations, replacing Ca^{2+} with respective ion properties. All ion conversion files are defined as [ion name]Accum.mod, where ion names are potassium or sodium.

Chloride concentrations in the extracellular space are calculated as the sum of sodium and potassium to maintain extracellular charge neutrality.

Stimulation Protocols

All stimulation protocols used in depolarizing the astrocyte are 10 pulses at 100 Hz to match experimental protocols [3]. Each stimulation was broken down as a 0.5 mM potassium increase that lasts for 0.5 ms unless stated otherwise. These extracellular potassium increases are confined to the extracellular space of the peripheral astrocyte, which is defined as the PAP. In the case of spillover experiments, this extracellular space is extended, resulting in a longer extracellular space affected by extracellular potassium increases.

Simulations and analyses

All models were implemented in NEURON, where the default astrocyte model was constructed using NEURON HOC version 8.2.0. Specific simulation programming was done by accessing the hoc object in the Python interface using custom code. MPICH [46] was used to parallelize individual simulations, using a custom code for repetitive simulations.

Statistics and reproducibility

Applied statistical tests are mentioned throughout the manuscript and/or figure captions. Briefly, comparison between constrained, spillover groups were done with one-way ANOVA while comparison of confined and spillover between specific KO conditions were done with paired t-test. All analyses were done using python code that is freely available.

References

[1] Takahiro Yaguchi and Tomoyuki Nishizaki. Extracellular high k+ stimulates vesicular glutamate release from astrocytes by activating voltage-dependent calcium channels. *Journal of cellular physiology*, 225(2):512–518, 2010.

[2] Oana Chever, Biljana Djukic, Ken D McCarthy, and Florin Amzica. Implication of kir4. 1 channel in excess potassium clearance: an in vivo study on anesthetized glial-conditional kir4. 1 knock-out mice. *Journal of Neuroscience*, 30(47):15769–15777, 2010.

[3] Moritz Armbruster, Saptarnab Naskar, Jacqueline P Garcia, Mary Sommer, Elliot Kim, Yoav Adam, Philip G Haydon, Edward S Boyden, Adam E Cohen, and Chris G Dulla. Neuronal activity drives pathway-specific depolarization of peripheral astrocyte processes. *Nature Neuroscience*, 25(5):607–616, 2022.

[4] Julian P Meeks and Steven Mennerick. Astrocyte membrane responses and potassium accumulation during neuronal activity. *Hippocampus*, 17(11):1100–1108, 2007.

[5] Biljana Djukic, Kristen B Casper, Benjamin D Philpot, Lih-Shen Chin, and Ken D McCarthy. Conditional knock-out of kir4. 1 leads to glial membrane depolarization, inhibition of potassium and glutamate uptake, and enhanced short-term synaptic potentiation. *Journal of Neuroscience*, 27(42):11354–11365, 2007.

[6] Robyn L O'Kane, Itziar Martınez-López, Mary R DeJoseph, Juan R Vina, and Richard A Hawkins. Na+-dependent glutamate transporters (eaat1, eaat2, and eaat3) of the blood-brain barrier: a mechanism for glutamate removal. *Journal of Biological Chemistry*, 274(45):31891–31895, 1999.

[7] Egor Byvaltcev, Mahraz Behbood, Jan-Hendrik Schleimer, Thomas Gensch, Alexey Semyanov, Susanne Schreiber, and Ulf Strauss. Kcc2 reverse mode helps to clear postsynaptically released potassium at glutamatergic synapses. *Cell Reports*, 42(8), 2023.

[8] Leonid P Savtchenko, Lucie Bard, Thomas P Jensen, James P Reynolds, Igor Kraev, Nikolay Medvedev, Michael G Stewart, Christian Henneberger, and Dmitri A Rusakov. Disentangling astroglial physiology with a realistic cell model in silico. *Nature communications*, 9(1):3554, 2018.

[9] Predrag Janjic, Dimitar Solev, and Ljupco Kocarev. Non-trivial dynamics in a model of glial membrane voltage driven by open potassium pores. *Biophysical Journal*, 2023.

[10] Baofeng Ma, Guangjin Xu, Wei Wang, John J Enyeart, and Min Zhou. Dual patch voltage clamp study of low membrane resistance astrocytes in situ. *Molecular Brain*, 7(1):1–12, 2014.

[11] Jessica McNeill, Christopher Rudyk, Michael E Hildebrand, and Natalina Salmaso. Ion channels and electrophysiological properties of astrocytes: implications for emergent stimulation technologies. *Frontiers in Cellular Neuroscience*, 15:644126, 2021.

[12] Jérémie Sibille, Khanh Dao Duc, David Holcman, and Nathalie Rouach. The neuroglial potassium cycle during neurotransmission: role of kir4. 1 channels. *PLoS computational biology*, 11(3):e1004137, 2015.

[13] Pei-Yu Shih, Leonid P Savtchenko, Naomi Kamasawa, Yulia Dembitskaya, Thomas J McHugh, Dmitri A Rusakov, Ryuichi Shigemoto, and Alexey Semyanov. Retrograde synaptic signaling mediated by k+ efflux through postsynaptic nmda receptors. *Cell reports*, 5(4):941–951, 2013.

[14] Peter H Chipman, Chi Chung Alan Fung, Alejandra Pazo Fernandez, Abhilash Sawant, Angelo Tedoldi, Atsushi Kawai, Sunita Ghimire Gautam, Mizuki Kurosawa, Manabu Abe, Kenji Sakimura, et al. Astrocyte GluN2C NMDA receptors control basal synaptic strengths of hippocampal CA1 pyramidal neurons in the stratum radiatum. *Elife*, 10:e70818, 2021.

[15] Noushin Ahmadpour, Meher Kantroo, Michael J Stobart, Jessica Meza-Resillas, Shahin Shabanipour, Jesus Parra-Nuñez, Tetiana Salamovska, Anna Muzaleva, Finnegan O'Hara, Dustin Erickson, et al. Cortical astrocyte n-methyl-d-aspartate receptors influence whisker barrel activity and sensory discrimination in mice. *Nature Communications*, 15(1):1571, 2024.

[16] Aparna Ravikrishnan, Pauravi J Gandhi, Gajanan P Shelkar, Jinxu Liu, Ratnamala Pavuluri, and Shashank M Dravid. Region-specific expression of nmda receptor glun2c subunit in parvalbumin-positive neurons and astrocytes: analysis of glun2c expression using a novel reporter model. *Neuroscience*, 380:49–62, 2018.

[17] Joselyn S Soto, Yasaman Jami-Alahmadi, Jakelyn Chacon, Stefanie L Moye, Blanca Diaz-Castro, James A Wohlschlegel, and Baljit S Khakh. Astrocyte–neuron subproteomes and obsessive–compulsive disorder mechanisms. *Nature*, 616(7958):764–773, 2023.

[18] Claudia Krebs, Herman B Fernandes, Claire Sheldon, Lynn A Raymond, and Kenneth G Baimbridge. Functional nmda receptor subtype 2b is expressed in astrocytes after ischemia in vivo and anoxia in vitro. *Journal of Neuroscience*, 23(8):3364–3372, 2003.

[19] Miroslav Gottlieb and Carlos Matute. Expression of ionotropic glutamate receptor subunits in glial cells of the hippocampal ca1 area following transient forebrain ischemia. *Journal of Cerebral Blood Flow & Metabolism*, 17(3):290–300, 1997.

[20] Keivan Moradi, Kamran Moradi, Mahin Ganjkhani, Mojtaba Hajihasani, Shahriar Gharibzadeh, and Gholamreza Kaka. A fast model of voltage-dependent

nmda receptors. *Journal of Computational Neuroscience*, 34:521–531, 2013.

[21] Xiaobing Chen, Christine Winters, Rita Azzam, Xiang Li, James A Galbraith, Richard D Leapman, and Thomas S Reese. Organization of the core structure of the postsynaptic density. *Proceedings of the National Academy of Sciences*, 105(11):4453–4458, 2008.

[22] Christian Henneberger, Lucie Bard, Aude Panatier, James P. Reynolds, Olga Kopach, Nikolay I. Medvedev, Daniel Minge, Michel K. Herde, Stefanie Anders, Igor Kraev, Janosch P. Heller, Sylvain Rama, Kaiyu Zheng, Thomas P. Jensen, Inmaculada Sanchez-Romero, Colin J. Jackson, Harald Janovjak, Ole Petter Ottersen, Erlend Arnulf Nagelhus, Stephane H.R. Oliet, Michael G. Stewart, U. Valentin Nägerl, and Dmitri A. Rusakov. LTP induction boosts glutamate spillover by driving withdrawal of perisynaptic astroglia. *Neuron*, 108:919–936.e11, 2020.

[23] Wolfgang Walz. Potassium homeostasis in the brain at the organ and cell level. *Advances in Molecular and Cell Biology*, 31:595–609, 2003.

[24] Tatsuya Kutsuwada, Nobuko Kashiwabuchi, Hisashi Mori, Kenji Sakimura, Etsuko Kushiya, Kazuaki Araki, Hiroyuki Meguro, Hisashi Masaki, Toshiro Kumanishi, Masaaki Arakawa, et al. Molecular diversity of the nmda receptor channel. *Nature*, 358(6381):36–41, 1992.

[25] T Kondoh, T Nishizaki, H Aihara, and N Tamaki. Nmda-responsible, apv-insensitive receptor in cultured human astrocytes. *Life sciences*, 68(15):1761–1767, 2001.

[26] P Aguilera et al. A metabotropic-like flux-independent nmda receptor regulates ca2+ exit from endoplasmic reticulum and mitochondrial membrane potential in cultured astrocytes. *Plos one*, 10(5):e0126314–e0126314, 2015.

[27] Annamaria Lia, Alessandro Di Spiezio, Lorenzo Vitalini, Manuela Tore, Giulia Puja, and Gabriele Losi. Ion channels and ionotropic receptors in astrocytes: Physiological functions and alterations in alzheimer ' s disease and glioblastoma. *Life*, 13(10):2038, 2023.

[28] Katarzyna Skowrońska, Marta Obara-Michlewska, Magdalena Zielińska, and Jan Albrecht. Nmda receptors in astrocytes: in search for roles in neurotransmission and astrocytic homeostasis. *International journal of molecular sciences*, 20(2):309, 2019.

[29] Mathieu Letellier, Yun Kyung Park, Thomas E. Chater, Peter H. Chipman, Sunita Ghimire Gautam, Tomoko Oshima-Takago, and Yukiko Goda. Astrocytes regulate heterogeneity of presynaptic strengths in hippocampal networks. *Proceedings of the National Academy of Sciences of the United States of America*, 113:E2685–E2694, 2016.

[30] Sónia Guerra-Gomes, Nuno Sousa, Luísa Pinto, and João F Oliveira. Functional roles of astrocyte calcium elevations: from synapses to behavior. *Frontiers in cellular neuroscience*, 11:427, 2018.

[31] Isabelle Latour, Jawed Hamid, Aaron M Beedle, Gerald W Zamponi, and Brian A Macvicar. Expression of voltage-gated ca2+ channel subtypes in cultured astrocytes. *Glia*, 41(4):347–353, 2003.

[32] Pierre Paoletti, Camilla Bellone, and Qiang Zhou. Nmda receptor subunit diversity: impact on receptor properties, synaptic plasticity and disease. *Nature Reviews Neuroscience*, 14(6):383–400, 2013.

[33] Jochen S Hub, Camilo Aponte-Santamaría, Helmut Grubmüller, and Bert L de Groot. Voltage-regulated water flux through aquaporin channels in silico. *Biophysical journal*, 99(12):L97–L99, 2010.

[34] Yutong Song and Eli Gunnarson. Potassium dependent regulation of astrocyte water permeability is mediated by camp signaling. *PLoS One*, 7(4):e34936, 2012.

[35] Yukihiro Ohno, Masato Kinboshi, and Saki Shimizu. Inwardly rectifying potassium channel kir4. 1 as a novel modulator of bdnf expression in astrocytes. *International journal of molecular sciences*, 19(11):3313, 2018.

[36] Audrey Denizot, Misa Arizono, U Valentin Nägerl, Hugues Berry, and Erik De Schutter. Control of ca2+ signals by astrocyte nanoscale morphology at tripartite synapses. *Glia*, 70(12):2378–2391, 2022.

[37] Nicholas T Carnevale and Michael L Hines. *The NEURON book*. Cambridge University Press, 2006.

[38] Elisabeth J van Bockstaele and Eric EO Colago. Selective distribution of the nmda-r1 glutamate receptor in astrocytes and presynaptic axon terminals in the nucleus locus coeruleus of the rat brain: an immunoelectron microscopic study. *Journal of Comparative Neurology*, 369(4):483–496, 1996.

[39] Man Yi Yim, Alexander Hanuschkin, and Jakob Wolfart. Intrinsic rescaling of granule cells restores pattern separation ability of a dentate gyrus network model during epileptic hyperexcitability. *Hippocampus*, 25(3):297–308, 2015.

[40] Bert Sakmann and Gerd Trube. Conductance properties of single inwardly rectifying potassium channels in ventricular cells from guinea-pig heart. *The Journal of physiology*, 347(1):641–657, 1984.

[41] Zhenjiang Yang, Haoxing Xu, Ningren Cui, Zhiqiang Qu, Sengthong Chanchevalap, Wangzhen Shen, and Chun Jiang. Biophysical and molecular mechanisms underlying the modulation of heteromeric kir4. 1–kir5. 1 channels by co2 and ph. *The Journal of general physiology*, 116(1):33–46, 2000.

[42] Ulyana Lalo, Yuri Pankratov, Frank Kirchhoff, R Alan North, and Alexei Verkhratsky. Nmda receptors mediate neuron-to-glia signaling in mouse cortical astrocytes. *Journal of Neuroscience*, 26(10):2673–2683, 2006.

[43] C Eo Jahr and CF Stevens. Glutamate activates multiple single channel conductances in hippocampal neurons. *Nature*, 325(6104):522–525, 1987.

[44] Niklas Hübel and Ghanim Ullah. Anions govern cell volume: a case study of relative astrocytic and neuronal swelling in spreading depolarization. *PloS one*, 11(3):e0147060, 2016.

[45] Mićo Božić, Samo Pirnat, Katja Fink, Maja Potokar, Marko Kreft, Robert Zorec, and Matjaž Stenovec. Ketamine reduces the surface density of the astroglial kir4. 1 channel and inhibits voltage-activated currents in a manner similar to the action of ba2+ on k+ currents. *Cells*, 12(10):1360, 2023.

[46] Message Passing Interface Forum. *MPI: A Message-Passing Interface Standard Version 4.1*, 2023.

[47] Anca R Rădulescu, Gabrielle C Todd, Cassandra L Williams, Benjamin A Bennink, Alex A Lemus, Haley E Chesbro, Justin R Bourgeois, Ashley M Kopec, Damian G Zuloaga, and Annalisa Scimemi. Estimating the glutamate transporter surface density in distinct sub-cellular compartments of mouse hippocampal astrocytes. *PLoS computational biology*, 18(2):e1009845, 2022.

[48] Michael Stegen, Florian Kirchheim, Alexander Hanuschkin, Ori Staszewski, Rüdiger W Veh, and Jakob Wolfart. Adaptive intrinsic plasticity in human dentate gyrus granule cells during temporal lobe epilepsy. *Cerebral cortex*, 22(9):2087–2101, 2012.

[49] Gerald Seifert, Kerstin Hüttmann, Devin K Binder, Christian Hartmann, Alexandra Wyczynski, Clemens Neusch, and Christian Steinhäuser. Analysis of astroglial K+ channel expression in the developing hippocampus reveals a predominant role of the kir4. 1 subunit. *Journal of Neuroscience*, 29(23):7474–7488, 2009.

[50] N. Spruston, P. Jonas, and B. Sakmann. Dendritic glutamate receptor channels in rat hippocampal CA3 and CA1 pyramidal neurons. *The Journal of Physiology*, 482:325–352, 1995.

[51] Richard J Clarke and Jon W Johnson. Voltage-dependent gating of nr1/2b nmda receptors. *The Journal of physiology*, 586(23):5727–5741, 2008.

[52] Shaul Hestrin, Pankaj Sah, and Roger A Nicoll. Mechanisms generating the time course of dual component excitatory synaptic currents recorded in hippocampal slices. *Neuron*, 5(3):247–253, 1990.

[53] M Korinek, M Sedlacek, O Cais, I Dittert, and L Vyklicky Jr. Temperature dependence of n-methyl-d-aspartate receptor channels and n-methyl-d-aspartate receptor excitatory postsynaptic currents. *Neuroscience*, 165(3):736–748, 2010.

[54] Nam-Kyung Kim and Hugh PC Robinson. Effects of divalent cations on slow unblock of native nmda receptors in mouse neocortical pyramidal neurons. *European Journal of Neuroscience*, 34(2):199–212, 2011.

[55] Dwight E Bergles and Craig E Jahr. Synaptic activation of glutamate transporters in hippocampal astrocytes. *Neuron*, 19(6):1297–1308, 1997.

[56] Min Zhou, Guangjin Xu, Minjie Xie, Xuexin Zhang, Gary P Schools, Liqun Ma, Harold K Kimelberg, and Haijun Chen. Twik-1 and trek-1 are potassium channels contributing significantly to astrocyte passive conductance in rat hippocampal slices. *Journal of Neuroscience*, 29(26):8551–8564, 2009.

[57] Alexei Verkhratsky and Maiken Nedergaard. Physiology of astroglia. *Physiological Reviews*, 98:239, 2018.

[58] Eric R Kandel, James H Schwartz, Thomas M Jessell, Steven Siegelbaum, A James Hudspeth, Sarah Mack, et al. *Principles of neural scienceKerchner2008,*, volume 4. McGraw-hill New York, 2000.

Acknowledgements

We thank Professor Yukiko Goda for helpful discussions throughout the project and her helpful feedback on the manuscript. We also thank Dr. Jules Lallouette, Dr. Maria Vazquez Pavon for helpful insights on our manuscript. This research has been funded by OISTGU and by JSPS KAKENHI grant number 24KJ2184.

Author Contributions

R.J.N. and E.D.S conceived the research. R.J.N. constructed the model with assistance from E.D.S.. R.J.N. wrote the original manuscript with suggestions from E.D.S..

Data availability

The data generated and/or analysed during the current study are available in the github repository, https://github.com/CNS-OIST/NEURONPAP.

Code availability

The custom Astrocyte NEURON model created in this study is freely available through modelDB, https://modeldb.science/2017008.

Supplementary Information

Supplementary Figs. 1 - 8, Supplementary Tables 1 - 8 and channel description.

Competing Interests

The authors have no competing interests to declare.